BRIEF COMMUNICATION www.jasn.org

Gli1$^+$ Pericyte Loss Induces Capillary Rarefaction and Proximal Tubular Injury

Rafael Kramann,*† Janewit Wongboonsin,‡§ Monica Chang-Panesso,‡ Flavia G. Machado,‡ and Benjamin D. Humphreys‡

*Renal Division, Brigham and Women's Hospital, Department of Medicine, Harvard Medical School, Boston, Massachusetts; †Division of Nephrology and Clinical Immunology, RWTH Aachen University Medical Faculty, RWTH Aachen University, Aachen, Germany; ‡Division of Nephrology, Department of Medicine, Washington University School of Medicine in St. Louis, St. Louis, Missouri; and §Department of Medicine, Siriraj Hospital, Mahidol University, Bangkok, Thailand

ABSTRACT

Peritubular capillary rarefaction is hypothesized to contribute to the increased risk of future CKD after AKI. Here, we directly tested the role of Gli1$^+$ kidney pericytes in the maintenance of peritubular capillary health, and the consequences of pericyte loss during injury. Using bigenic Gli1-CreER^{t2}; R26tdTomato reporter mice, we observed increased distance between Gli1$^+$ pericytes and endothelial cells after AKI (mean±SEM: 3.3±0.1 μm before injury versus 12.5±0.2 μm after injury; $P<0.001$). Using a genetic ablation model, we asked whether pericyte loss alone is sufficient for capillary destabilization. Ten days after pericyte ablation, we observed endothelial cell damage by electron microscopy. Furthermore, pericyte loss led to significantly reduced capillary number at later time points (mean±SEM capillaries/high-power field: 67.6±4.7 in control versus 44.1±4.8 at 56 days; $P<0.05$) and increased cross-sectional area (mean±SEM: 21.9±0.4 μm^2 in control versus 24.1±0.6 μm^2 at 10 days; $P<0.01$ and 24.6±0.6 μm^2 at 56 days; $P<0.001$). Pericyte ablation also led to hypoxic focal and subclinical tubular injury, reflected by transient expression of Kim1 and vimentin in scattered proximal tubule segments. This analysis provides direct evidence that AKI causes pericyte detachment from capillaries, and that pericyte loss is sufficient to trigger transient tubular injury and permanent peritubular capillary rarefaction.

J Am Soc Nephrol 28: 776–784, 2017. doi: 10.1681/ASN.2016030297

Up to 20% of patients that develop AKI will go on to develop late stage CKD, and these patients are at increased risk of ESRD and death.[1,2] Understanding the mechanisms underlying this epidemiologic link is a priority, with a strong focus being on the structural alterations that occur in kidney after an episode of AKI.[3–6] One hypothesis is that AKI causes detachment of pericytes from peritubular endothelial cells, triggering endothelial injury, capillary rarefaction, hypoxia and, ultimately, fibrosis with CKD progression.[7,8] Direct evidence in support of this hypothesis is lacking because of the absence of specific markers for kidney pericytes that would allow unambiguous fate tracing and genetic ablation in mouse models.

We recently reported that Gli1 marks a perivascular population of mesenchymal stem cell-like cells that form an extensive network from the arterial adventitia in the pericyte niche.[9] Genetic fate tracing experiments revealed that these perivascular Gli1$^+$ cells are a major source of kidney myofibroblasts and can be targeted therapeutically.[9,10] In this study, we sought experimental evidence for detachment of Gli1$^+$ cells from peritubular capillaries after AKI, and whether pericyte loss is sufficient to induce peritubular capillary loss and altered morphology.

We genetically labeled pericytes using Gli1-CreER^{t2} mice crossed against the R26tdTomato reporter mouse (Gt(ROSA)26Sor$^{tm9(CAF\text{-}tdTomato)Hze/J}$; Figure 1A). After tamoxifen injection, mice were subjected to severe unilateral ischemia reperfusion injury (IRI; 28-minute clamp). The injury was induced 10 days after tamoxifen injection to eliminate the possibility of recombination after injury. Mice were euthanized 5 days after IRI. We performed endothelial cell staining (with CD31) and quantitatively measured the distance of tdTomato$^+$ cells to the nearest endothelial cell by generating distance maps in ImageJ (Figure 1, B and C, Supplemental Material).

Received March 14, 2016. Accepted August 9, 2016.

R.K. and J.W. contributed equally to this work.

Published online ahead of print. Publication date available at www.jasn.org.

Correspondence: Dr. Benjamin D. Humphreys, Division of Renal Disease, Washington University School of Medicine, 660 South Euclid Avenue, CB 8129, St. Louis, MO 63110, or Dr. Rafael Kramann, Division of Nephrology and Clinical Immunology, Rheinisch-Westfälische Technische Hochschule Aachen University, Pauwelstrasse 30, 52074 Aachen, Germany. Email: humphreysbd@wustl.edu or rkramann@gmx.net

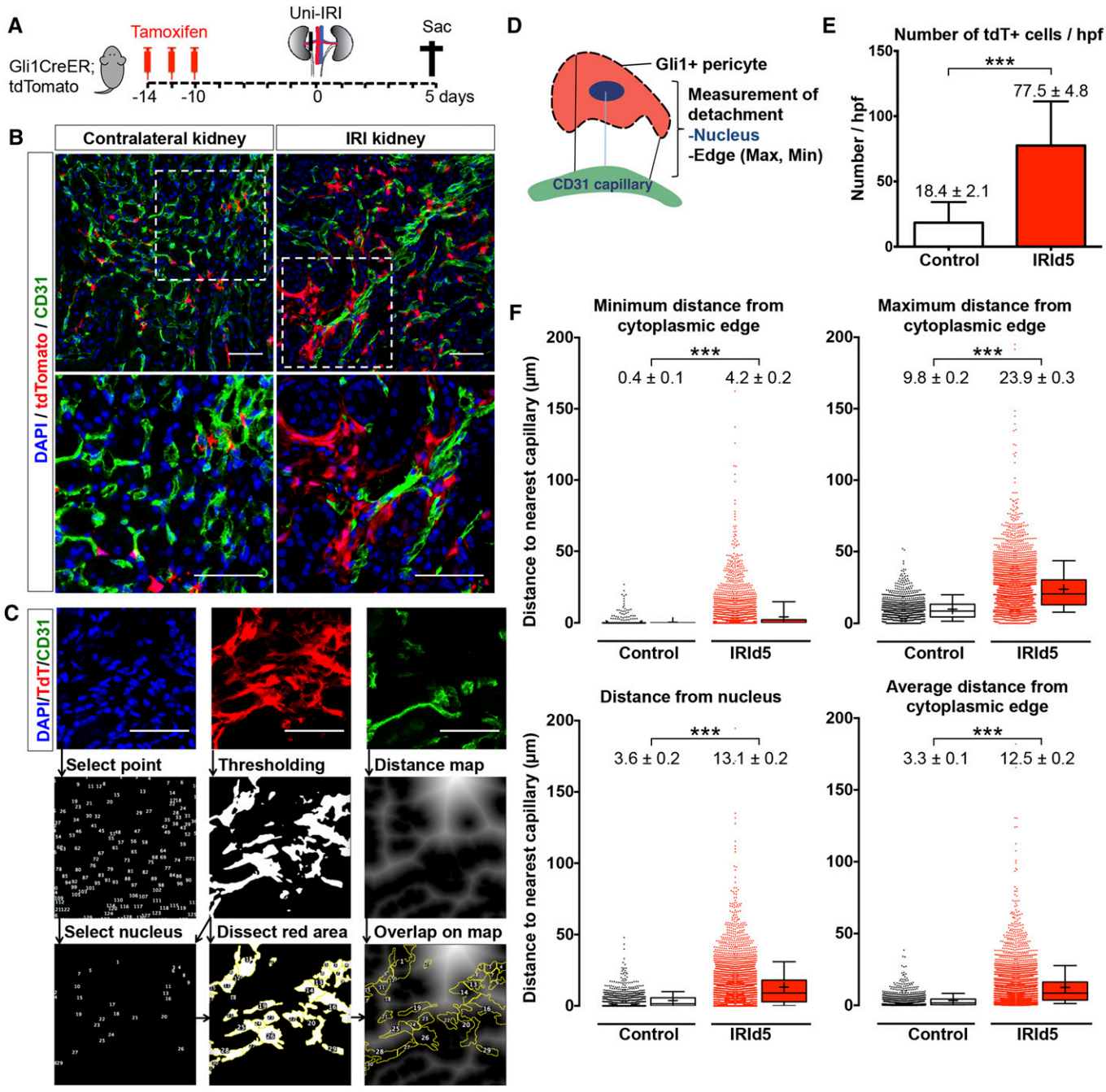

Figure 1. Gli1$^+$ pericytes detach from endothelial cells and expand after IRI. (A) Gli1$^+$ cells were genetically tagged using bigenic Gli1-CreER^{t2}; R26tdTomato mice. Tamoxifen was administered and mice underwent severe unilateral IRI 10 days after the last tamoxifen dose and were euthanized 5 days after surgery. (B) Representative images of CD31-stained kidneys from Gli1-CreER^{t2}; R26tdTomato mice at day 5 after IRI. (C) Representative images of distance analysis indicating detachment of pericytes from endothelial cells. Immunofluorescence images of three channels (DAPI, tdTomato, and CD31) were split. Points of maximum intensity of each nucleus were selected and merged with tdTomato$^+$ to mark the nucleus of the Gli1$^+$ pericyte. Selected nuclei and tdTomato$^+$ area were overlaid on the distance map generated from with the CD31 image to measure the distance of nuclei and cytoplasmic edges to the endothelial cells. (D) Scheme of pericyte–endothelial distance measurement. (E) Quantification of tdTomato$^+$ cell number after IRI. (F) Measured distances from tdTomato$^+$ pericytes to the closest endothelial cells indicating detachment after injury. Of note, data represent n=11 mice, six female and five male, in the contralateral kidney group and n=10 mice, five female and five male, in the severe IRI group; mean±SEM in E and F; box and whiskers with 10th–90th percentiles in F; + indicates mean in F; ***$P<0.001$, by t-test; all scale bars are 50 μm. DAPI, 4′,6-diamidino-2-phenylindole.

We detected increased numbers of tdTomato$^+$ cells (mean±SEM: 18.4±2.2 versus 77.5±4.8 cells/high-power field [hpf]; $P<0.001$) after IRI, as expected (Figure 1, B and E). Importantly the distance of tdTomato$^+$ cells to the closest endothelial cell increased significantly (Figure 1, D and F). We measured an increase of the minimum as well as maximum distance from the cytoplasmic edge (minimum distance: 0.4±0.1–4.2±0.2 μm; $P<0.001$; maximum distance: 9.8±0.2–23.9±0.3 μm; $P<0.001$) or the nucleus (3.6±0.2–13.1±0.2 μm; $P<0.001$) of the tdTomato$^+$ pericyte to the closest endothelial cell (Figure 1F). We next asked whether undifferentiated Gli1$^+$ pericytes (tdTomato$^+$/αSMA$^-$) and Gli1-derived myofibroblasts (tdTomato$^+$/αSMA$^+$) both show increased distance from endothelial cells after injury. Indeed, we observed increased distances of both tdTomato$^+$/αSMA$^-$ cells and tdTomato$^+$/αSMA$^+$ cells to the closest endothelial cells, after IRI (Supplemental Figure 1), suggesting that myofibroblast differentiation is not a requirement for pericyte detachment from capillaries after injury.

In addition to detachment of pericytes, we also detected peritubular capillary rarefaction after IRI (Supplemental Figure 2). Pericyte–endothelial cell crosstalk has been investigated after kidney injury, and experiments by Lin *et al.* using Col1α1-GFP mice have suggested that pericytes migrate away from capillaries after kidney injury.[11] However, the lack of a specific kidney pericyte marker that would allow inducible genetic fate tracing has prevented experimental proof of pericyte migration from capillaries *in vivo*.[11,12]

Our data indicates that Gli1$^+$ myofibroblast progenitors detach from capillaries after injury. The proximity of pericytes and endothelial cells to one another is likely crucial for the signaling that stabilizes peritubular capillaries.[13] Whether pericyte loss itself is sufficient to induce capillary destabilization, however, remains unresolved. An alternative hypothesis is that primary endothelial damage causes secondary pericyte detachment, not the other way around.

To address the functional consequences of pericyte loss, we asked whether cell-specific genetic ablation of Gli1$^+$ cells would trigger endothelial damage and capillary rarefaction. We crossed Gli1-CreER^{t2}; R26tdTomato mice to R26iDTR mice. Tamoxifen administration in bigenic mice leads to heritable expression of the human diphtheria toxin (DTX) receptor in Gli1$^+$ pericytes and perivascular cells. After tamoxifen-induced recombination and a 10-day washout period, DTX was administered to specifically ablate Gli1$^+$ pericytes (Figure 2A). Mice were euthanized at 10 days or 56 days after the first DTX dose. We observed evidence of endothelial injury by electron microscopy upon pericyte ablation at day 10, consisting of swollen endothelial mitochondria with loss of cristae, thickening of capillary basement membrane, and denudation of endothelial cells from the capillary basement membrane (Figure 2D). To quantify peritubular capillary changes after pericyte ablation, we applied fluorescence microangiography (FMA) high-resolution imaging combined with our automated MATLAB-based analysis of peritubular capillary size and density (Figure 2B, Supplemental Material).[3] As a positive control, we used triple transgenic Gli1-CreER^{t2}; iDTR; R26tdTomato mice to demonstrate successful depletion of Gli1$^+$ cells after DTX administration (Figure 2C).

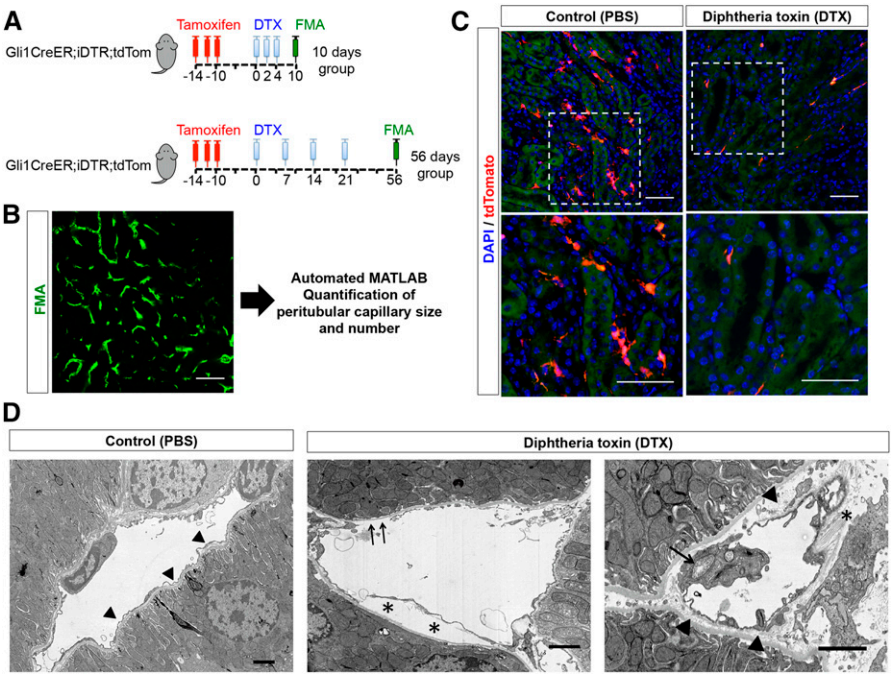

Figure 2. Cell-specific genetic ablation of Gli1$^+$ cells in healthy mice. (A) Experimental scheme: Gli1-CreER^{t2}; iDTR; R26tdTomato trigenic mice were administered tamoxifen. Heritable expression of DTX receptor was induced in Gli1$^+$ cells. DTX was given to specifically ablate Gli1$^+$ cells as indicated, and the mice were followed and euthanized 10 days or 56 days after the first DTX dose. Control animals were given vehicle instead of DTX. (B) Random images of kidneys after FMA were taken (n=5/kidney section) and analyzed with our MATLAB-based script. (C) Gli1-CreER^{t2}; iDTR; R26tdTomato trigenic mice were administered tamoxifen and received DTX or vehicle (PBS) to validate ablation of tdTomato$^+$ cells. (D) Evidence of endothelial injury after Gli1$^+$ pericyte ablation. Left panel, normal peritubular capillary. Note the very thin endothelial cytoplasm surrounding basement membrane (arrowheads). Center panel, injured endothelial cell with delamination of cell from basement membrane (asterisks) and areas of denuded basement membrane (arrows). Right panel, an injured endothelial cell with swollen cytoplasm and mitochondrial exhibiting disrupted cristae (arrow). Accumulation of electron-lucent material in between the endothelial cell and the capillary basement membrane is evident (arrowheads). Collagen fibers can be seen (asterisk). Scale bars are 50 μm in immunofluorescence images and 2 μm in electron microscopy images. DAPI, 4′,6-diamidino-2-phenylindole.

Gli1$^+$ pericyte ablation led to a gradual decline in cortical capillary number (Figure 3, A and D). Total area and total number of capillaries were significantly lower compared with the control group at 56 days (mean±SEM: 1478±104–1084±149 μm^2/hpf; P=0.03, and 67.6±4.7–44.1±4.8 capillaries/hpf; P=0.001). Further analysis revealed a shift in capillary size distribution with a substantial rarefaction of small capillaries (<15 μm^2; Figure 3B). In contrast to our previous IRI experiments, where we observed a biphasic trend with an increased number of small capillaries and a drop in the number of larger capillaries,[3] pericyte ablation triggered more prominent rarefaction of the smaller capillaries (Figure 3B). Interestingly, we observed an increase in capillary cross-sectional area from 21.9±0.4 to 24.1±0.6 μm^2 at 10 days (P=0.01) and 24.6±0.6 μm^2 at 56 days after DTX injection (P=0.004; Figure 3C). This might be explained by the predominant rarefaction of smaller capillaries, resulting in a shift toward a larger mean of the capillary cross-sectional area. We limited analysis to capillaries with an area >4.9 μm^2 because it has been previously reported that this is the lower size limit of capillaries through which erythrocytes can pass.[3,14] To exclude larger vessels, we used an upper cut-off value of 100 μm^2 as previously reported.[3] Analysis of capillary number using standard CD31-based staining yielded a similar trend (Supplemental Figure 2B). Similar to the effect on cortical microvasculature, Gli1 cell ablation also induced a capillary rarefaction in the outer medulla (Supplemental Figure 3).

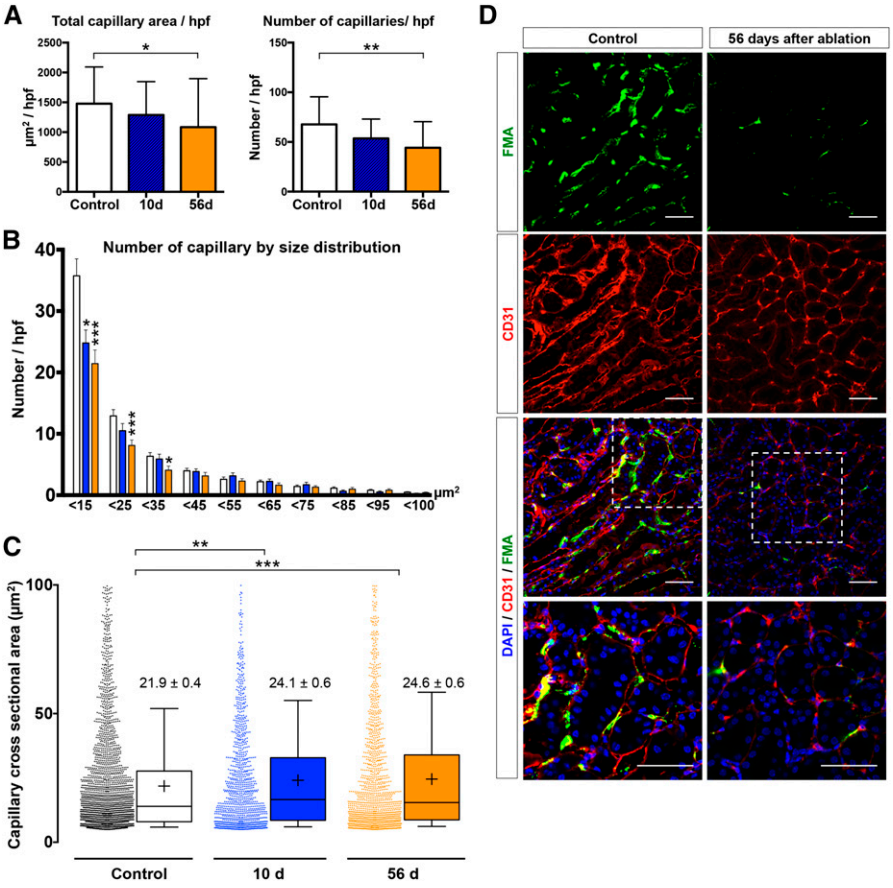

Figure 3. Analysis of cortical microvasculature depicted by FMA reveals capillary rarefaction after Gli1$^+$ pericyte ablation. (A) Ablation of Gli1$^+$ pericytes resulted in reduction of total capillary cross-sectional area (control: 1478±104 μm^2, 10 days: 1289±124.6 μm^2, and 56 days: 1084±148.6 μm^2) and total number of capillaries (control: 67.6±4.7 capillaries/hpf, 10 days: 53.6±4.4 capillaries/hpf, and 56 days: 44.1±4.8 capillaries/hpf; mean±SEM, *t*-test). (B) Gli1$^+$ pericyte ablation had the highest effect on small capillaries with a significant reduction in capillaries smaller than 15, 25, and 35 μm^2. (C) The individual cortical capillary cross-sectional area increased slightly after pericyte ablation (data shown in mean±SEM; box and whiskers with 10th–90th percentiles; + indicates mean; one-way ANOVA with *post hoc* Bonferroni correction). (D) Representative images of FMA and CD31 staining at 56 days after pericyte ablation versus vehicle (scale bars are 50 μm). Of note, data represent n=7 mice in control, n=4 mice in 10 days group and n=6 in 56 days group; *P<0.05; **P<0.01; ***P<0.001. DAPI, 4′,6-diamidino-2-phenylindole.

We next asked whether pericyte ablation caused parenchymal damage. Quantitative real-time PCR showed an 18-fold increase in Kidney Injury Molecule 1 (Kim1) mRNA level at 10 days after ablation (Figure 4A). Kim1 protein expression also significantly increased and was located in focal proximal tubular segments cells positive for Lotus tetragonolobus lectin (Figure 4, A and B). These Kim1-expressing tubular epithelial cells were also positive for vimentin, indicating their dedifferentiation (Figure 4C), and several were proliferating, as indicated by costaining for the cell cycle marker Ki67 (Supplemental Figure 3A).[15] Intriguingly, Kim1 mRNA and protein were absent by 56 days, suggesting that proximal tubule damage induced by pericyte loss was fully repaired by this time point. Electron microscopy at 10 days after Gli1$^+$ cell ablation confirmed focal tubular epithelial injury (Figure 4D). Kidney sections stained with periodic acid–Schiff also showed focal areas of tubular injury at 10 days after injury, with a repair at 56 days (Supplemental Figure 4B). Because of the focal nature of this tubular epithelial injury, blindly scored random hpfs (400×, five per kidney) did not show a significant injury (Supplemental Figure 4B).

We next asked whether the tubular injury might be explained by hypoxia as a consequence of capillary rarefaction. We repeated the short term ablation experiment in bigenic Gli1-CreER^{t2}; iDTR mice (n=5 vehicle versus n=7 DTX) and injected the mice with the hypoxia

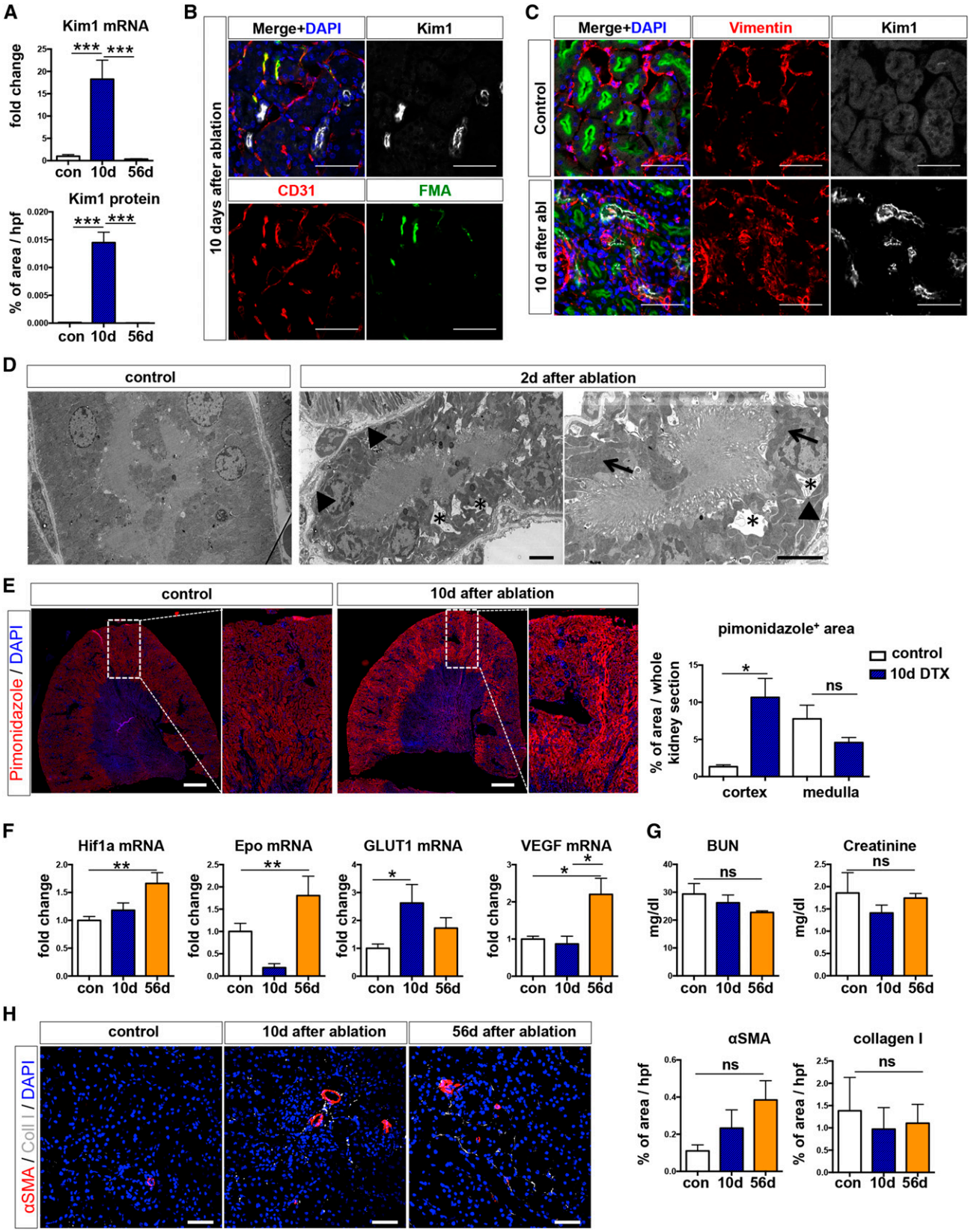

Figure 4. Ablation of Gli1$^+$ pericytes causes transient proximal tubular injury. (A) Increased Kim1 mRNA and protein expression at 10 days after Gli1$^+$ cell ablation (***$P<0.001$; one-way ANOVA with *post hoc* Bonferroni correction). (B, C) Scattered Kim1 expression in proximal tubular (costained with Lotus tetragonolobus lectin [LTL]) brush borders. We observed increased Kim1 expression in areas with reduced

marker pimonidazole at 24 hours before euthanizing. We clearly observed increased pimonidazole staining in focal areas with Kim1 tubular epithelial injury (Supplemental Figure 4C) and significantly increased cortical pimonidazole-positive area size in scanned whole kidney sections (Figure 4E). Furthermore, we observed a significant mRNA expression of the hypoxic response genes Hif1a, erythropoietin, GLUT1, and VEGF, suggesting that Gli1$^+$ cell ablation indeed resulted in kidney hypoxia (Figure 4F). Kidney functional parameters, such as BUN and creatinine, were not affected by Gli1$^+$ cell ablation (Figure 4G).

Selective tubular injury has been reported to induce tubulointerstitial fibrosis.[16] We therefore asked whether pericyte ablation triggering capillary rarefaction and tubular injury might, in fact, induce tubulointerstitial fibrosis. Indeed, we observed a very mild fibrotic response with increased mRNA expression of collagen IαI (Supplemental Figure 4D). Staining and quantification of both collagen I and αSMA protein expression did not show a significant increase after Gli1 cell ablation (Figure 4H). Because we have previously reported that Gli1$^+$ cells are a major source of kidney myofibroblasts,[9] Gli1$^+$ cell ablation might also affect the development of fibrosis, despite tubular injury inducing interstitial fibrosis.

Interestingly, Gli1$^+$ cell ablation also resulted in an inflammatory response, with upregulation of renal TNFα and IL6 mRNA expression (Supplemental Figure 4E). Renal collagen IV and TGFβ1 mRNA expression did not significantly change after Gli1 cell ablation (Supplemental Figure 4, F and G).

Gli1$^+$ pericytes represent a subpopulation of interstitial kidney cells that exhibit mesenchymal stem cell properties and are a major source of renal myofibroblasts after injury. Although ablation of these cells during kidney fibrosis (unilateral ureteral obstruction) ameliorated fibrosis,[9] we demonstrate here that ablation of these cells during homeostasis causes focal and transient proximal tubular injury with sustained peritubular capillary rarefaction. Depletion of pericytes is a well described phenomenon during early nonproliferative diabetic retinopathy,[17,18] which leads to endothelial dysfunction. Conditional knockout of several genes, such as NG2, in pericytes, has also been reported to result in endothelial dysfunction.[19] The mechanism driving proximal tubular injury after pericyte depletion is most likely through capillary rarefaction resulting in cortical hypoxia. Pericytes have also been reported to have direct interaction with other cells, such as epithelial cells, and coordinate endothelial–epithelial communication.[20] Recently, Lemos *et al.* reported that genetic ablation of FoxD1$^+$ cells in bigenic FoxD1Cre; iDTR mice resulted in AKI with abrupt increase of serum creatinine, BUN, albuminuria, and capillary rarefaction.[21] This much more severe injury might be explained by the fact that FoxD1Cre also recombines in all vascular smooth muscle cells, mesangial cells, and a minor fraction of tubular epithelial cells.[22] The milder injury we observed in our experiments is likely explained by the fact that FoxD1 marks all interstitial pericytes, whereas Gli1$^+$ cells represent a small subfraction of interstitial PDGFRβ^+ pericytes, and Gli1 is not expressed in the mesangium, vascular smooth muscle, or epithelium.

Gli1$^+$ cells, similar to other pericytes, primarily localize to the corticomedullary junction.[8,9,23] Our observation of cortical tubular injury distant from the outer medulla after Gli1$^+$ cell ablation suggests that peritubular damage is capable of inducing damage in remote tubule segments. Similar observations have been made in proximal tubules, where tubular epithelial damage causes later glomerulosclerosis. We speculate that rarefaction of the peritubular blood supply, which feeds the entire nephron, might explain these distant effects.

In conclusion, we demonstrate, using inducible genetic fate tracing, that Gli1$^+$ pericytes detach from capillaries after kidney injury and Gli1$^+$ pericyte depletion induces capillary rarefaction and proximal tubular injury. This indicates that a therapeutic strategy eliminating Gli1$^+$ pericytes during CKD may have the unwanted effect of destabilizing the peritubular capillary network. More targeted inhibition of pericyte–myofibroblast differentiation or myofibroblast expansion, steps that occur after pericyte detachment, might be a more favorable therapeutic strategy.

CONCISE METHODS

All mouse experiments followed the animal experimental guidelines issued by the Animal Care and Use Committee at Washington University. Gli1-CreER^{t2} (*i.e.,* Gli1$^{tm3(re/ERt2)alj}$/J; stock no. 007909), R26tdTomato (*i.e.,* B6-Cg-Gt(ROSA)26Sor$^{tm(CAG-tdTomato)Hze}$/J; stock no. 007900), and iDTR mice (*i.e.,* C57BL/6-Gt(ROSA)26Sor$^{tm1(HBEGF)Awai}$/J; stock no. 007900) were purchased from Jackson

FMA perfusion. Scale bars are 50 μm. (C) Injured tubules expressed vimentin indicating dedifferentiation of tubular epithelial cells. Scale bars are 50 μm. (D) Evidence of tubular injury by electron microscopy at 10 days after Gli1$^+$ cell ablation. Asterisks indicate irregular intracytoplasmic vacuolization, arrowheads indicate simplification and thickening of the basal membrane, and arrows indicate enlargement and bulging of mitochondria. Scale bars are 4 μm. (E) Representative images and quantification of pimonidazole staining in kidneys of bigenic Gli1-CreER^{t2}; iDTR mice at 10 days after ablation (n=5 control/vehicle, n=7 DTX). *$P<0.05$ by t-test, scale bars are 100 μm. (F) Upregulation of hypoxic response genes after Gli1 cell ablation. *$P<0.05$; **$P<0.01$ by one-way ANOVA with *post hoc* Bonferroni. (G) Gli1 ablation did not affect serum BUN or creatinine. (H) Representative images and quantification of collagen 1 and αSMA indicating no significant change after Gli1$^+$ cell ablation. Scale bars are 50 μm. NS, not significant. DAPI, DAPI, 4′,6-diamidino-2-phenylindole.

Laboratories (Bar Harbor, ME). Offspring were genotyped by PCR according to the protocol from Jackson Laboratories. For lineage tracing, Gli1-CreER^{t2}; R26tdTomato bigenic mice were given three doses of 0.4 mg/g body wt tamoxifen in corn oil/3% ethanol (Sigma-Aldrich, St. Louis, MO) *via* oral gavage, 10 days before IRI. IRI was performed as previously described.[24] Briefly, mice were anesthetized with pentobarbital sodium (60 mg/kg body wt, administered intraperitoneally) and buprenorphine was used for pain control (0.1 mg/kg body wt, administered intraperitoneally). Incisions were made by flank incision, exposing the kidneys, and ischemia was induced by clamping the renal pedicle with nontraumatic microaneurysm clamps (Roboz, Rockville, MD) for 28 minutes (for severe IRI). Contralateral kidneys were left undisturbed. Reperfusion was visually verified. Body temperatures were controlled at 36.5°C–37.5°C throughout the procedure. A total of 1 ml of normal saline was administered subcutaneously, after the surgery. For ablation experiments, bigenic Gli1-CreER^{t2}; iDTR mice received tamoxifen, as previously mentioned. After a 10-day washout period, DTX (Peprotech) dissolved in PBS (Gibco, Carlsbad, CA) at the dose of 50 ng/g body wt was given intraperitoneally, as indicated (Figure 2A). Control mice received an intraperitoneal injection of PBS. To validate the cell ablation, triple transgenic mice (Gli1-CreER^{t2}; iDTR; R26tdTomato) were generated and treated with the same protocol as the bigenic group. Mice were euthanized 10 days and 56 days after administration of the first dose of DTX. FMA was performed at death. For detection of hypoxia, pimonidazole (Hypoxyprobe-1 kit) was injected at 60 mg/kg body wt intraperitoneally, at 24 hours before euthanizing. Staining was achieved using rabbit anti-pimonidazole antibody at 1:100 (PAb2627AP; Hypoxyprobe). Quantification of positive area was performed as percentage of the whole cortex or outer medulla in a scanned whole kidney section, using NIS Elements (Nikon, Tokyo, Japan). Quantification of collagen 1 and αSMA staining was done in five random hpfs per kidney (400×), as percentage of positive area, using NIS Elements (Nikon). Quantification of tubular injury was performed in five random hpf images of kidney sections stained with periodic acid–Schiff, using the following injury score: 0, 0%–5%; 1, 5%–10%; 2, 11%–25%; 3, 26%–45%; 4, 46%–75%; and 5, 76%–100% for tubular atrophy, dilation, protein casts, necrotic cells, and brush border loss. BUN and creatinine was measured by HPLC at the University of Alabama at Birmingham - University of California at San Diego O'Brien Core Center for Acute Kidney Injury Research.

Real-Time PCR Experiments

Tissue or cell pellets were harvested and immediately snap frozen in liquid nitrogen. RNA from kidneys was extracted according to the manufacturer instructions, using the RNeasy Mini Kit (Qiagen, Germantown, MD), and 600 ng of total RNA was reverse transcribed with iScript (Bio-Rad, Hercules, CA). Quantitative PCRs were carried out with iQ-SYBR Green supermix (Bio-Rad) and the Bio-Rad CFX96 Real Time System with the C1000 Touch Thermal Cycler. Cycling conditions were 95°C for 3 minutes, then 40 cycles of 95°C for 15 seconds and 60°C for 1 minute, followed by one cycle of 95°C for 10 seconds. Glyceraldehyde-3-phosphate dehydrogenase (GAPDH) was used as a housekeeping gene. Data were analyzed using the $2^{-\Delta\Delta ct}$ method. The following primers were used: GAPDH: forward 5′-AGGTCGGTGTGAACGGATTTG-3′; reverse 5′-TGTAGACCATGTAGTTGAGGTCA-3′; αSMA: forward 5′-CTGACAGAGGCAC CACTGAA-3′, reverse 5′-CATCTCCAGAGTCCAGCACA-3′; Col1α1: forward 5′-TGAC TGGAAGAGCGGAGAGT-3′, reverse 5′-GTTCGGGCTGATGTACCAGT-3′; EPO: forward 5′-GTGGAAGAACAGGCCATAGAA-3′, reverse 5′-GTCTATATGAAGCTGAAGGGTCTC-3′; HIF1a1: forward 5′- CGGCGAGAACGAGAAGAAAAAG-3′, reverse 5′-TGGGGAAGTG GCAACTGATG-3′; TGFβ1: forward 5′-GGAGCAACATGTGGAACTCTA-3′, reverse 5′-CAGCCACTCAGGCGTATC-3′; VEGF: forward 5′-TCATGCGGATCAAACCTCAC-3′, reverse 5′-TCTGGCTTTGTTCTGTCTTTCT-3′; KIM1: forward 5′-AAACCAGAGATTCCCACACG-3′, reverse 5′-GTCGTGGGTCTTCCTGTAGC-3′; Col4a1: forward 5′-GGGAGAGAAAGGTGCTGTG-3, reverse 5′-TGCCAGGTAAGCCGTTA AAT-3′; Glut1: forward 5′-TCTGTCGGCCTCTTTGTTAATC-3′, reverse 5′-CCAGTTTGGAGAAGCC CATAA-3′; TNFα: forward 5′-CTATGTCTCAGCCTCTTCT CATTC-3′, reverse 5′-GAGGC CATTTGGGAACTTCT-3′; IL6: forward 5′-CTTCACAAGTCGG AGGCTTAAT-3′, reverse 5′-GCAAGTG CATCATCGTTGTTC-3′.

Electron Microscopy

Kidneys were fixed by Karnovsky fixative. Then, samples were quartered and sliced into approximately 1.5-mm thick pieces, rinsed in cacodylate buffer three times for 10 minutes each, and subjected to a secondary fixation for 1 hour in 1% osmium tetroxide/0.3% potassium ferrocyanide in cacodylate buffer on ice. Then, samples were washed in ultrapure water three times for 10 minutes each, and stained *en bloc* for 1 hour with 2% aqueous uranyl acetate. After staining was complete, samples were briefly washed in ultrapure water, dehydrated in a graded acetone series (50%, 70%, 90%, 100%, ×2) for 10 minutes in each step, and infiltrated with microwave assistance (Pelco BioWave Pro, Redding, CA) into LX112 resin. Samples were cured in an oven at 60°C for 48 hours. Once the resin was cured, blocks were trimmed to a face extending from the outer membrane to the outer stripe of the outer medulla. Sections (70-nm thin) were then taken and imaged on an FE-SEM (Zeiss Crossbeam 540, Oberkochen, Germany) using the aSTEM detector. The FE-SEM was operated at 28 KeV with a probe current of 1.1 nA, and STEM detector was operated with the annular rings inverted for additional sample contrast.

FMA

At the time of organ harvest, mice were anesthetized with pentobarbital (60 mg/kg of body wt, administered intraperitoneally). FMA was performed as previously described.[3] Briefly, an incision was made at the midline toward the lateral thoracic cage. A 27-gauge butterfly catheter was inserted into left ventricle, followed by infusion of prewarmed 41°C solutions, as follows: 1 ml of heparinized saline (100 IU/ml heparin; Sagent Pharmaceuticals), 1 ml of 3 M KCl, 10 ml of PBS, and 5 ml of agarose-fluorescent microbead mixture (1% low-melting-point agarose, stock no. 50080; Lonza) in distilled water with 0.02 μm FluoSpheres sulfate (yellow-green, stock no. F8845; Invitrogen, Carlsbad, CA) or 0.06 μm Dragon green Carboxylated Polystyrene beads (stock no. FC02F–11587; Bangs Laboratories) The inferior vena cava was cut before the infusion of PBS. After perfusion of fluorescent beads, organs were placed

on ice for 10 minutes to solidify agarose. Then, they were placed in 4% paraformaldehyde on ice for 2 hours, 30% sucrose in PBS at 4°C overnight, and embedded in optimum cutting temperature compound (Sakura Finetek).

Immunofluorescence

Tissue sections were cut at 7-μm thickness and mounted on Superfrost slides (Thermo Fisher Scientific, Vernon Hills, IL). Sections were washed with PBS (three times, 5 minutes each), then blocked with 10% normal goat serum (Vector Laboratories, Burlingame, CA), permeabilized with 0.2% Triton-X100 in PBS, and then stained with primary antibody specific for rat anti-CD31 (1:100, stock no. 14–0311; eBioscience, San Diego, CA), FITC-conjugated anti-Lotus tetragonolobus lectin (1:200, stock no. FL-1321; Vector Laboratories), rabbit anti-vimentin (1:100; stock no. ab92547; Abcam, Inc., Cambridge, MA), goat anti-KIM1 (1:200, stock no. AF1817; R&D Systems, Minneapolis, MN), mouse anti-αSMA (1:200, stock no. A2457; Sigma-Aldrich) and rabbit anti-Ki67 (1:100, stock no. VP-RM04; Vector Laboratories). Secondary antibodies included FITC-, Cy3, or Cy5-conjugated (Jackson ImmunoResearch Laboratories, West Grove, PA). Then, sections were stained with 4′,6′-diamidino-2-phenylindole and mounted in Prolong Gold (Life Technologies, Carlsbad, CA). Images were obtained by confocal microscopy (Nikon C1 Eclipse and C2$^+$ Eclipse; Nikon). Five images of the outer cortex and five images of the outer stripe of the outer medulla were taken randomly at 400× magnification, using the same laser power and gain intensity for all pictures.

Distance Quantification by ImageJ

Random images from the outer stripe of the outer medulla were analyzed. All images were automatically processed by ImageJ (Figure 1C). First, all images were split into RGB channels. Gaussian blur was applied to adjust background noise in all channels. Autothreshold was used to convert intensity values of CD31 staining and tdTomato$^+$ area into binary data. Then a distance map was created from the binary data of CD31. One maximum intensity point was selected as the representative point of each nucleus. These points were used to divide the binary tdTomato$^+$ area into smaller areas representing single tdTomato$^+$ cells. Selected nuclei and the divided tdTomato$^+$ areas were overlayed on a CD31-generated distance map. The script is provided in Supplemental Material. We used αSMA immunostaining to separate tdTomato cells into αSMA$^+$ and αSMA$^-$ cells. Distance from nucleus and cytoplasmic edges of these two subsets to the nearest vessel were calculated as mentioned above.

Image Quantification by MATLAB

For quantification of peritubular capillary size and diameter, we utilized the same MATLAB script we have described previously.[3] The script removes background noise, generates a binary image of capillaries, and provides data of capillary size, number, and diameter.

Statistical Analyses

Data were presented as mean±SEM. ANOVA with *post hoc* Bonferroni correction was used for multiple group comparison. Student *t*-test was used to compare two different groups. GraphPad Prism software, version 6.0c (GraphPad Software Inc., San Diego, CA) and SPSS version 22 were used for statistical analysis. P value < 0.05 was considered a statistical significant difference.

ACKNOWLEDGMENTS

Electron microscopy was performed, in part through the use of the Washington University Center for Cellular Imaging.

This work was supported by the National Institutes of Health (NIH)/National Institute of Diabetes and Digestive and Kidney Diseases grants DK107274, DK103740, and DK103050, and by an Established Investigator Award of the American Heart Association (all to B.D.H); by a Start grant of the Rheinisch-Westfälische Technische Hochschule Aachen University (101/15), a grant of the Deutsche Forschungsgemeinschaft (KR 4073/3-1), a grant of the European Research Council (ERC-StG 677448), and a grant of the State of North Rhine-Westphalia (all to R.K.); and by a Prince Mahidol Award-Youth Program scholarship and fellowship from the Faculty of Medicine at Siriraj Hospital, Mahidol University (to J.W.). We also acknowledge support from the University of Alabama at Birmingham-University of California at San Diego O'Brien Core Center for Acute Kidney Injury Research (NIH grant P30-DK079337).

DISCLOSURES

None.

REFERENCES

1. Amdur RL, Chawla LS, Amodeo S, Kimmel PL, Palant CE: Outcomes following diagnosis of acute renal failure in U.S. veterans: focus on acute tubular necrosis. *Kidney Int* 76: 1089–1097, 2009
2. Coca SG, Singanamala S, Parikh CR: Chronic kidney disease after acute kidney injury: a systematic review and meta-analysis. *Kidney Int* 81: 442–448, 2012
3. Kramann R, Tanaka M, Humphreys BD: Fluorescence microangiography for quantitative assessment of peritubular capillary changes after AKI in mice. *J Am Soc Nephrol* 25: 1924–1931, 2014
4. Kramann R, Dirocco DP, Maarouf OH, Humphreys BD: Matrix Producing Cells in Chronic Kidney Disease: Origin, Regulation, and Activation. *Curr Pathobiol Rep* 1: 301–311, 2013
5. Basile DP: Rarefaction of peritubular capillaries following ischemic acute renal failure: a potential factor predisposing to progressive nephropathy. *Curr Opin Nephrol Hypertens* 13: 1–7, 2004
6. Basile DP, Donohoe D, Roethe K, Osborn JL: Renal ischemic injury results in permanent damage to peritubular capillaries and influences long-term function. *Am J Physiol Renal Physiol* 281: F887–F899, 2001
7. Schrimpf C, Duffield JS: Mechanisms of fibrosis: the role of the pericyte. *Curr Opin Nephrol Hypertens* 20: 297–305, 2011
8. Kramann R, Humphreys BD: Kidney pericytes: roles in regeneration and fibrosis. *Semin Nephrol* 34: 374–383, 2014
9. Kramann R, Schneider RK, DiRocco DP, Machado F, Fleig S, Bondzie PA, Henderson JM, Ebert BL, Humphreys BD: Perivascular Gli1+ progenitors are key contributors to injury-induced organ fibrosis. *Cell Stem Cell* 16: 51–66, 2015
10. Kramann R, Fleig SV, Schneider RK, Fabian SL, DiRocco DP, Maarouf O, Wongboonsin J, Ikeda Y, Heckl D, Chang SL, Rennke HG, Waikar SS, Humphreys BD: Pharmacological GLI2 inhibition prevents myofibroblast cell-cycle progression and reduces kidney fibrosis. *J Clin Invest* 125: 2935–2951, 2015
11. Lin SL, Chang FC, Schrimpf C, Chen YT, Wu CF, Wu VC, Chiang WC, Kuhnert F, Kuo CJ, Chen YM, Wu KD, Tsai TJ, Duffield JS: Targeting endothelium-pericyte cross talk by

inhibiting VEGF receptor signaling attenuates kidney microvascular rarefaction and fibrosis. *Am J Pathol* 178: 911–923, 2011
12. Schrimpf C, Teebken OE, Wilhelmi M, Duffield JS: The role of pericyte detachment in vascular rarefaction. *J Vasc Res* 51: 247–258, 2014
13. Armulik A, Abramsson A, Betsholtz C: Endothelial/pericyte interactions. *Circ Res* 97: 512–523, 2005
14. Henquell L, LaCelle PL, Honig CR: Capillary diameter in rat heart in situ: relation to erythrocyte deformability, O2 transport, and transmural O2 gradients. *Microvasc Res* 12: 259–274, 1976
15. Kusaba T, Lalli M, Kramann R, Kobayashi A, Humphreys BD: Differentiated kidney epithelial cells repair injured proximal tubule. *Proc Natl Acad Sci U S A* 111: 1527–1532, 2014
16. Grgic I, Campanholle G, Bijol V, Wang C, Sabbisetti VS, Ichimura T, Humphreys BD, Bonventre JV: Targeted proximal tubule injury triggers interstitial fibrosis and glomerulosclerosis. *Kidney Int* 82: 172–183, 2012
17. Hill J, Rom S, Ramirez SH, Persidsky Y: Emerging roles of pericytes in the regulation of the neurovascular unit in health and disease. *J Neuroimmune Pharmacol* 9: 591–605, 2014
18. Ejaz S, Chekarova I, Ejaz A, Sohail A, Lim CW: Importance of pericytes and mechanisms of pericyte loss during diabetes retinopathy. *Diabetes Obes Metab* 10: 53–63, 2008
19. You WK, Yotsumoto F, Sakimura K, Adams RH, Stallcup WB: NG2 proteoglycan promotes tumor vascularization via integrin-dependent effects on pericyte function. *Angiogenesis* 17: 61–76, 2014
20. Kaissling B, Le Hir M: The renal cortical interstitium: morphological and functional aspects. *Histochem Cell Biol* 130: 247–262, 2008
21. Lemos, DR, Marsh, G, Huang, A, Campanholle, G, Aburatani, T, Dang, L, Gomez, IG, Fisher, K, Ligresti, G, Peti-Peterdi, J, Duffield, JS: Maintenance of vascular integrity by pericytes is essential for normal kidney function [published online ahead of print June 26, 2016]. *Am J Physiol Renal Physiol* doi:10.1152/ajprenal.00030.2016
22. Kobayashi A, Mugford JW, Krautzberger AM, Naiman N, Liao J, McMahon AP: Identification of a multipotent self-renewing stromal progenitor population during mammalian kidney organogenesis. *Stem Cell Rep* 3: 650–662, 2014
23. Fabian SL, Penchev RR, St-Jacques B, Rao AN, Sipilä P, West KA, McMahon AP, Humphreys BD: Hedgehog-Gli pathway activation during kidney fibrosis. *Am J Pathol* 180: 1441–1453, 2012
24. Humphreys BD, Valerius MT, Kobayashi A, Mugford JW, Soeung S, Duffield JS, McMahon AP, Bonventre JV: Intrinsic epithelial cells repair the kidney after injury. *Cell Stem Cell* 2: 284–291, 2008

See related editorial, "Pericytes Preserve Capillary Integrity to Prevent Kidney Hypoxia," on pages 717–719.

This article contains supplemental material online at http://jasn.asnjournals.org/lookup/suppl/doi:10.1681/ASN.2016030297/-/DCSupplemental.